

Article

Manganese Molybdenum Oxide Micro Rods Adorned Porous Carbon Hybrid Electrocatalyst for Electrochemical Determination of Furazolidone in Environmental Fluids

Sivakumar Musuvadhi Babulal ¹, Tse-Wei Chen ^{1,2,3}, Shen-Ming Chen ^{1,*}, Wedad A. Al-Onazi ⁴ and Amal M. Al-Mohaimeed ^{4,*}

¹ Electroanalysis and Bioelectrochemistry Lab, Department of Chemical Engineering and Biotechnology, National Taipei University of Technology, No. 1, Section 3, Chung-Hsiao East Road, Taipei 106, Taiwan; mbsiva94@gmail.com (S.M.B.); twchenchem@gmail.com (T.-W.C.)

² Research and Development Center for Smart Textile Technology, National Taipei University of Technology, No. 1, Section 3, Chung-Hsiao East Road, Taipei 106, Taiwan

³ Department of Materials, Imperial College London, London SW72AZ, UK

⁴ Department of Chemistry, College of Science, King Saud University, P.O. Box 22452, Riyadh 11495, Saudi Arabia; walonazi@ksu.edu.sa

* Correspondence: smchen78@ms15.hinet.net (S.-M.C.); muhemeed@ksu.edu.sa (A.M.A.-M.)



Citation: Babulal, S.M.; Chen, T.-W.; Chen, S.-M.; Al-Onazi, W.A.; Al-Mohaimeed, A.M. Manganese Molybdenum Oxide Micro Rods Adorned Porous Carbon Hybrid Electrocatalyst for Electrochemical Determination of Furazolidone in Environmental Fluids. *Catalysts* **2021**, *11*, 1397. <https://doi.org/10.3390/catal1111397>

Academic Editor: Edward G. Gillan

Received: 29 October 2021

Accepted: 16 November 2021

Published: 18 November 2021

Publisher's Note: MDPI stays neutral with regard to jurisdictional claims in published maps and institutional affiliations.



Copyright: © 2021 by the authors. Licensee MDPI, Basel, Switzerland. This article is an open access article distributed under the terms and conditions of the Creative Commons Attribution (CC BY) license (<https://creativecommons.org/licenses/by/4.0/>).

Abstract: The frequent occurrence of furazolidone (FZD) in environmental fluids reveals the ongoing increase in use and raises concerns about the need of monitoring it. To investigate the electrochemical behavior of FZD, a novel sensor of manganese molybdenum oxide (MMO) micro rods adorned three-dimensional porous carbon (PC) electrocatalyst was constructed. The crystalline structure and surface morphology of the MMO/PC composite was characterized by XRD, Raman, FESEM, and HR-TEM. Electrochemical impedance spectroscopy (EIS), cyclic voltammetry (CV), and amperometric(i-t) methods were used to assess the electrocatalytic activity of modified electrodes. In the presence of FZD, the as-fabricated MMO/PC modified glassy carbon electrode (GCE) performed better at lower potentials with a greater peak current than other modified GCE. These results emanate from the synergistic effect of the MMO/PC suspension on the GCE. The electrochemical behavior of the amperometric(i-t) technique was used to determine FZD. Amperometric(i-t) detection yielded linear dynamic ranges of 150 nM to 41.05 µM and 41.05 to 471.05 µM with detection limits of 30 nM. The MMO/PC hybrid sensor was also effectively used to detect FZD in environmental fluids, yielding ultra-trace level detection.

Keywords: furazolidone; manganese molybdenum oxide micro rods; porous carbon; cyclic voltammetry; amperometric(i-t) method

1. Introduction

Furazolidone, 3-(5-nitrofurfurylideneamino)-2-oxazolidinone, is a class of nitrofuran, which are Schiff's base derivatives of nitrofuraldehyde. It can be used to treat ulcers and gastrointestinal diseases which are triggered by bacteria and protozoa. However, some research has suggested that furazolidone has pathogen infection in poultry, pigs, rabbits, fish, and human health [1,2]. The economically farmed animals' death is prevented by furazolidone and it is illegally added to animal food in most of the countries [3,4]. Hence, the environmental level of usage must be monitored with highly sensitive techniques for the detection of residual furazolidone. Regular detecting approaches for the detection of furazolidone include high-performance liquid chromatography (HPLC) [5], high-performance liquid chromatography-tandem mass spectrometry (HPLC-MS) [6], enzyme-linked immunosorbent assays (ELISAs) [7], spectrophotometry [8], and electrochemical methods [9]. Even though these methods have some benefits such as high sensitivity and accuracy, they also have disadvantages, such as being expensive, stability issues, interference issues, and

being tedious [10,11]. When compared to the other methods, an electrochemical sensor is an alternative one, which is low-cost, simple to process, with elevated sensitivity and superior reproducibility, and is appropriate for real-time monitoring [12,13].

The electrochemical analysis has covered the measurement of electrical values as well as their connection to chemical variables. Electrochemical analysis has been applied in industrial quality control, environmental research, and medical analysis. In addition, electrodes have played a crucial role in electrochemical oxidation and reduction processes [14,15], particularly in their effect on electron transport between electroactive species and the electrode surface. Electrochemical behaviors for many types of electroactive substances on the surfaces of different electrodes could be seen. By varying the size and chemical composition of the electrode surface, the analytical performance may be enhanced by attaining electrocatalytic characteristics, such as hypersensitivity and selectivity [16,17]. Chemically modified electrodes would make use of the characteristics of the modifier reagents to tackle a variety of electrochemical issues. Because of their exceptional characteristics, micro rods and hybrid composites have a wide range of uses, particularly in electrode modification for electrochemical sensing [18,19].

Recently, porous carbon has been utilized for electrocatalyst materials, due to their spectacular property such as porous structure, chemical stability, plenteous conductivity, and large specific surface area for ion adsorption. Among these properties include engineering of the pore structures with a higher electrochemical accessible surface area, faster electron-transport path, and a more robust interface with the electrolyte and electrode surface [20,21]. Therefore, it has been considered as an innovative advanced material to find utility in multiple applications related to the catalyst [22,23], electronic [24], supercapacitors [25], medicines [26], and electrochemical sensor [27].

Metal molybdates are a family of inorganic materials that have gotten a lot of interest recently because of their widespread use in fields like lithium storage [28], HER [29], hybrid devices [30], luminescence property [31], and heavy metal detection sensors [32]. In particular, MnMoO₄ has received special attention due to its inexpensive cost, exceptional stability, outstanding chemical properties, low toxicity, and abundant oxidation, as well as the original price state of Mo and Mn compared to that of binary transition metal oxides such as FeMoO₄ [33], CuMoO₄ [34], NiMoO₄ [35], CoMoO₄ [36], and others. Thus, manganese molybdate (MnMoO₄) as a superior electrocatalytic electrode material has an electrochemical application.

Despite the performance during electrochemical redox reactions, it has portrayed very low conductivity and instability of the electron transfer rate. To get rid of this issue, combining MnMoO₄ with highly conductive carbonaceous material (such as carbon nanotubes, nanofibers, nanocarbon, and porous carbon) could portray enhanced electrical conductivity as well the electrochemical activity of the reduction reaction. Currently, the use of binary transition metal oxide decorated carbon hybrid electrocatalysts is expanding the electrochemical sensing sector. Among these, hybrid electrocatalysts have a larger active electrode surface area, improved electrochemical amplification signal, lower potential with higher current, superior sensitivity, and electrode durability. Recently, a binary transition metal oxide hybrid composite was developed with higher electrochemical performance and used various fields of application. Li et al. designed a Ni(OH)₂/MnMoO₄ composite on reduced graphene oxide/Ni foam utilized for battery/supercapacitor hybrid device [37]. Hussain et al. fabricated binder-free 2D-hexagonal CoMoO₄ nanosheets used for pseudocapacitor application [38]. Zhang et al. reported a MgH₂–MnMoO₄ rod composite for improvement of hydrogen storage energy [39]. Venkatesh et al. constructed a MnMoO₄/GNS electrocatalyst used for ecological pollutant detection [40]. Ranjith et al. reported an electrochemical sensing platform with simultaneous detection of 1D–2D MnMoO₄–MXene nanocomposites and modified GCE [41]. In that order, we developed co-precipitation synthesis of MnMoO₄ micro rods at the initial stage. Then, the synthesized MnMoO₄ micro rods were treated with 3D network porous carbon through the ultrasonication process. The crystalline structure and surface morphology of ultrasonication-assisted MnMoO₄ micro rods in assembled

porous carbon composites were examined. The as-prepared MMO/PC (1:3 ratio) hybrid electrocatalyst modified GC electrode exhibited significantly enhanced electrocatalytic performance in the detection of furazolidone. The as-prepared MMC/PC hybrid electrocatalyst revealed lower electron transfer resistance, excellent stability, selectivity, good sensitivity, and optimum environmental samples with recoveries.

2. Results and Discussion

The simple co-precipitation technique was used to architect MnMoO₄ micro rods. X-ray diffraction analysis confirmed the crystal structure of MMO, porous carbon, and MMO/PC composite powder. As depicted in Figure 1A, XRD patterns show architected MMO (a), porous carbon (b), and MMO/PC composite (c) samples. The diffraction peaks of as-prepared MMO shows clearly the monoclinic phase of pure crystal structure with space group C2/m. The measured diffraction peaks and interplanar spacing matched the typical MMO diffraction pattern (JCPDS card no: 01-072-0285) [42]. All the observed major diffraction peaks at 2θ values of 12.8° , 18.7° , 22.7° , 24.7° , 25.7° , 25.9° , 27.7° , 31.2° , 34.2° , 35.7° , 37.9° , 39.0° , 42.8° , 45.5° , 51.2° , 53.4° , 57.0° , 58.3° , and 59.3° were indexed to the lattice planes (100), (-201), (021), (201), (220), (002), (-311), (112), (311), (400), (-132), (-113), (-332), (-403), (-204), (004), (024), (620), and (-424), respectively. Among them, the XRD pattern of porous carbon has been verified to the two sharp and distinctive diffraction peaks at 2θ values of 25.1° and 42° , which correspond to plane values (002) and (100), respectively [43]. The XRD patterns of the MMO/PC composite have exhibited no change when compared to the diffraction patterns of pure MMO. Aside from a small peak shift, the intensity has been reduced, indicating confirmation of the composite.

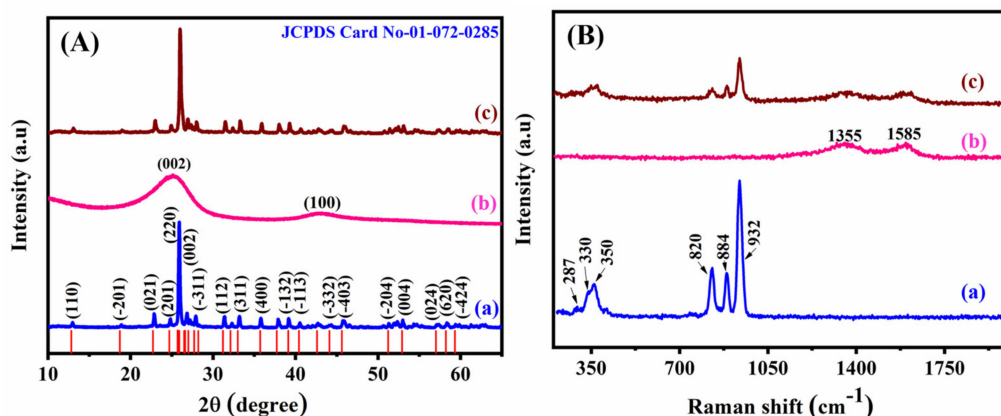


Figure 1. (A,B) Crystal structure analysis and Raman spectra of (a) MMO, (b) porous carbon, and (c) MMO/PC composite.

Raman spectroscopy is used to determine the bonding nature, defect, and vibration states of metal oxide on the surface. The structure of MMO (a), porous carbon (b), and the as-prepared MMO/PC composite (c) were further revealed by Raman spectroscopy, as shown in Figure 1B. The Raman active bands detected at 932 , 884 , 820 , 350 , 330 , and 287 cm^{-1} are representative bands for MMO [44]. The stretching vibrations and bending vibrations of tetrahedral MoO_4^{2-} ions are attributed to the higher and lower wavenumber frequency region. In addition, the porous carbon exhibited two peaks at (D-band) 1355 cm^{-1} and (G-band) 1585 cm^{-1} , respectively [45]. The D-band is associated with crystal defects and the disordered nature of porous carbon. The G-band is ascribed to the tangential stretching (E_{2g}) mode of graphite. It provides robust evidence that carbon is present in the MMO/PC composite (Figure 1B(c)). Finally, all the above-mentioned Raman active bands were present in the as-prepared MMO/PC composite.

The chemical state of elements in the as-fabricated MMO/PC composite was analyzed by XPS measurement. The wide scan survey revealed the presence of elements Mn 2p, Mo 3d, O 1s, and C 1s. They can be seen in Figure 2A. In Figure 2B the high-

resolution core-level spectrum of Mn 2p is displayed which can be deconvoluted into the four peaks. The main binding energy of the Mn 2p_{3/2} occurred at 641.14 eV and Mn 2p_{1/2} at 653.26 eV, respectively [46]. The main binding energy of Mn 2p_{3/2} and 2p_{1/2} are separated by 11.6 eV, which corresponds to the Mn²⁺ oxidation state. The chemical state of the Mo 3d core-level spectrum (Figure 2C) was deconvoluted into two binding energy values at 232 and 235 eV corresponding to Mo 3d_{5/2} and Mo 3d_{3/2}, respectively, which reveals the MoO₄⁻ oxidation state [46]. The O 1s binding energy peak was observed at 529 and 530 eV [47], which belongs to the oxygen species of chemisorbed and the hydroxyl group of surface adsorbed water molecules. The state of C 1s binding energy values at 284.1, 285.1, and 28.6 eV are assigned to C–C, C=C, and C–O respectively [48]. Based on the XPS result, the novel MMO/PC composite chemical state elements are confirmed.

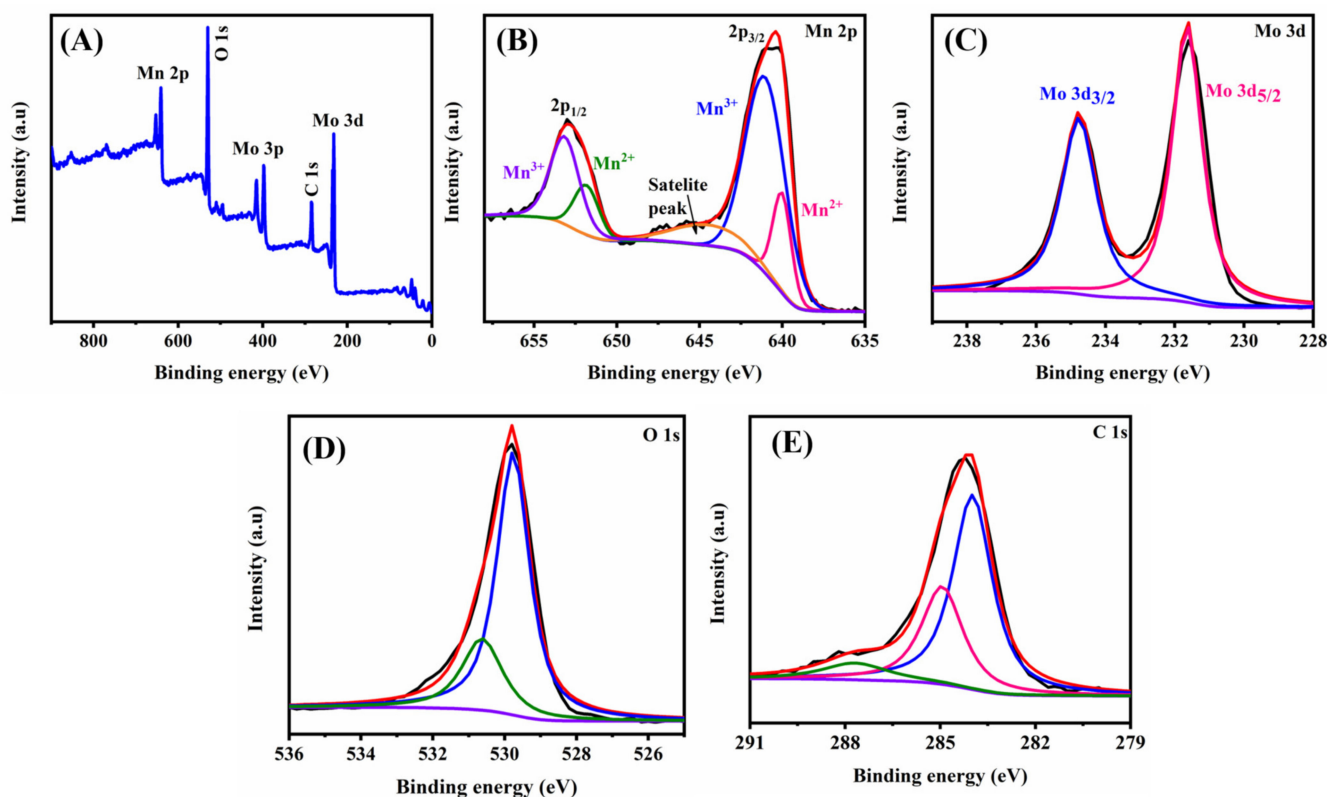


Figure 2. (A) Overall survey of presenting an element of Mn 2p, Mo 3d, O 1s, and C 1s, and (B–E) XPS spectra of as-prepared MMO/PC composite.

The surface morphology of as-prepared MMO, porous carbon, and as-fabricated MMO/PC composite were examined by FESEM images and are presented in Figure 3. As shown in Figure 3A,B, the formation of the micro rod-like structures of MMO can be observed at a lower magnification view in the range of 1 μ m. From this view, the other structure formation has not been produced, it confirms the formation of pure micro rods MMO particles in this study. In the higher magnification view growth of micro rods has larger and thicker arrays, as seen in Figure 3C. In addition, the large and uniform 3D porous structures like carbon morphology were observed in the higher and lower magnification view image, which can be seen in Figure 3D,E. Structurally, this three-dimensional hole-like structure has been used to interconnect with electrode materials, it could serve to enhance electron transfer performance. As shown in Figure 3F–H, as-fabricated MMO/PC portrays higher composite surface morphology and lower angles can be observed. The as-synthesized MMO enriched with a three-dimensional interconnected porous carbon hybrid electrocatalyst could increase the electrochemical rate performance. More importantly, EDS

and elemental mapping confirmed the presence of each element, Mn, Mo, O, and C in Figure 3I–N.

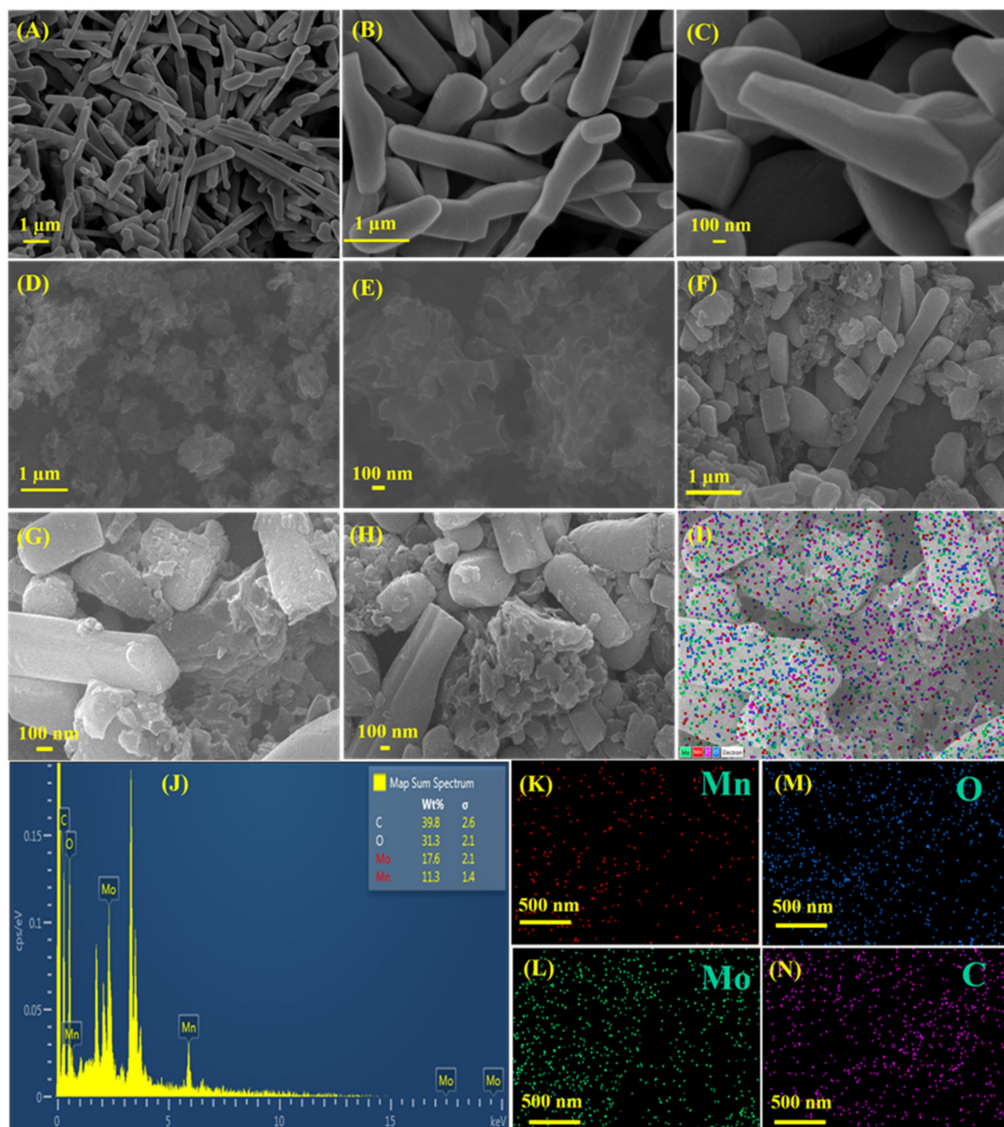


Figure 3. FESEM images of (A–C) as-prepared MMO, (D,E) porous carbon, (F–I) as-prepared MMO/PC composite, (J) EDS analysis, and (K–N) elemental mapping of confirmed Mn, Mo, O, and C elements.

Further, information about the internal structure of as-fabricated MMO/PC composite was obtained from HR-TEM, as shown in Figure 4. As illustrated in Figure 4A,B, it clearly shows as-synthesized micro rods structure formation. The porous carbon nature exhibits hole-like 3D porous structure formation, as demonstrated in Figure 4C. The novel properties of one-dimensional micro rods and three-dimensional porous carbon hybrid composite at different angle views are depicted in Figure 4D–G. The 3D porous carbon has the merits of high surface area, fast electron transfer path, and higher conductivity. As stated earlier, novel properties are connected with micro to enhance the electrochemical activity of the modified composite electrode. From the SAED pattern, the as-synthesized MMO single-crystal nature was confirmed, as shown in Figure 4H. The crystal and amorphous layer can be seen and the lattice fringe, as shown in Figure 4I.

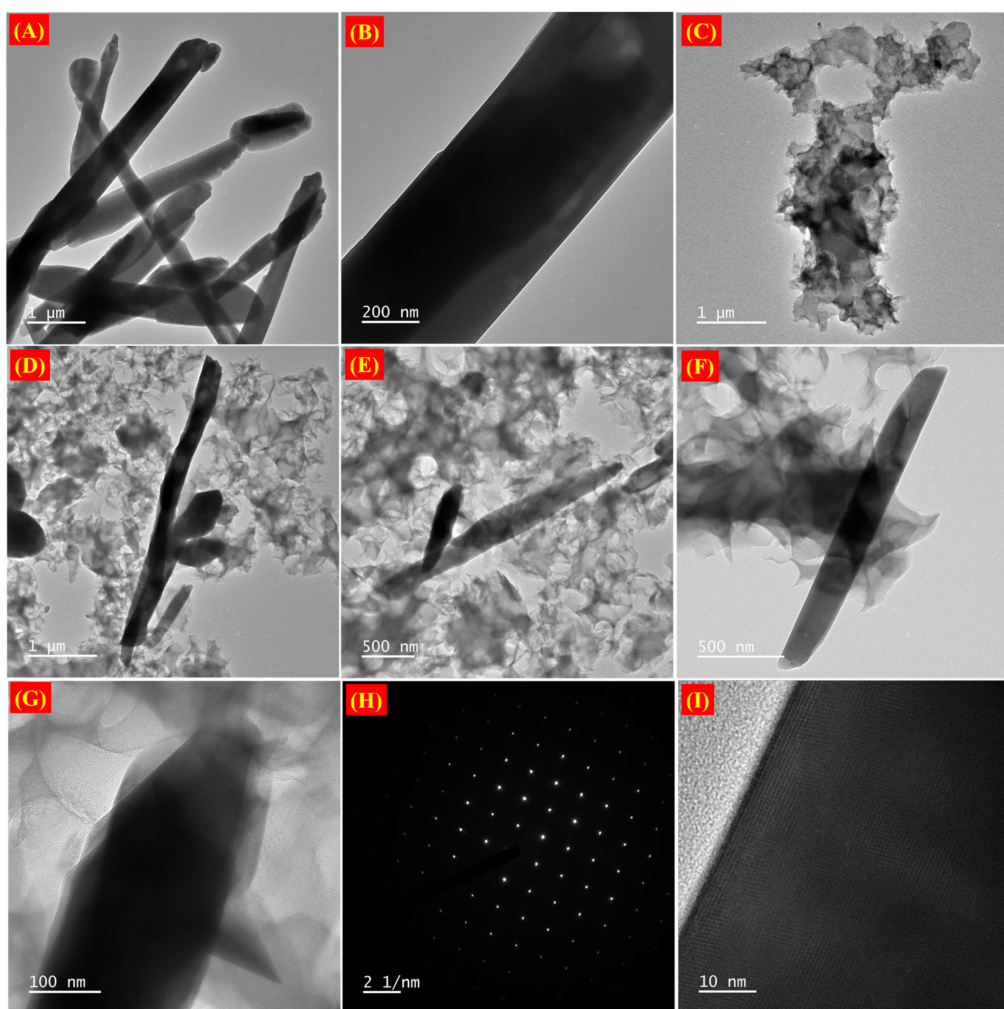


Figure 4. HR-TEM images of (A,B) MMO, (C) porous carbon (D–G) as-prepared MMO/PC composite, (H,I) SAED pattern, and lattice fringes of the as-prepared MMO/PC composite.

2.1. Electrochemical Characterization and Application

To investigate electrochemical properties of electron transfer resistance (R_{ct}) of different modified electrodes, electrochemical impedance spectroscopy was performed. From EIS data results, the semicircle occurred at a higher frequency and linear curve at a lower frequency region. As shown in Figure 5A, Nyquist plot of the (a) bare/GCE, (b) MMO/GCE, (c) porous carbon/GCE, and (d) MMO/PC/GCE, the calculated R_{ct} values are 364, 2301, 93, and $58\ \Omega$, respectively. The inset in Figure 5A shows that the EIS measurement revealed the Randles circuit model which describes the electrical network at the modified electrodes. The obtained R_{ct} value can be seen, the as-prepared MMO/PC/GCE exhibited a much smaller charge transfer resistance value than bare, MMO and porous carbon/GCE. The results exhibited the as-prepared MMO/PC/GCE has excellent conductivity and enhances fast charge transfer processes.

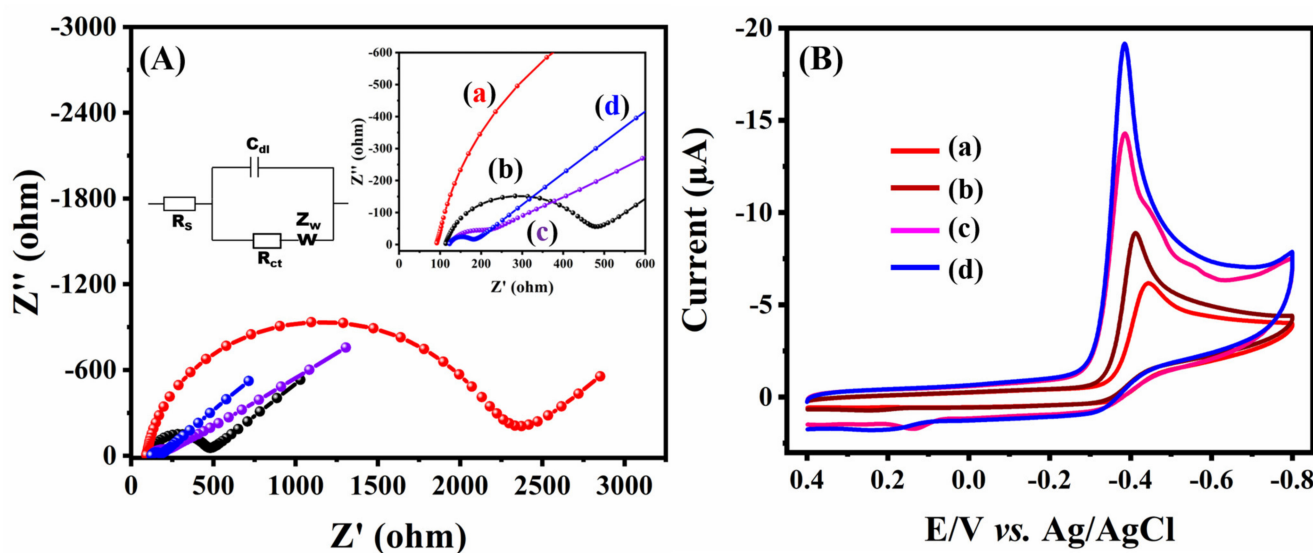


Figure 5. (A) EIS spectra of the (a) bare/GCE, (b) MMO/GCE, (c) porous carbon/GCE, and (d) as-prepared MMO/PC/GCE measured in electrolyte solution of 5 mM $[\text{Fe}(\text{CN})_6]^{3-/4-}$ with 0.1 M KCl. (B) CVs measurement of (a) bare/GCE, (b) MMO/GCE, (c) porous carbon/GCE and (d) MMO/PC/GCE at a sweep rate 50 mV/s in presence of 100 μM (0.01 M) FZD.

The investigation of the electrocatalytic activity of the catalytic material was performed with cyclic voltammetry. As shown in Figure 5B, the bare/GCE (a), MMO/GCE (b), porous carbon/GCE (c), and (d) MMO/PC/GCE in the presence of (0.01 M) 100 μM FZD were recorded at a sweep rate of 50 mV/s in PBS (pH 7). In the presence of 100 μM FZD at various modified electrodes, the cathodic peak current and peak potential at (-0.44 V , $-6.0 \mu\text{A}$) for bare/GCE, (-0.41 V , $-8.82 \mu\text{A}$) for MMO/GCE, (-0.38 V , $-14.2 \mu\text{A}$) for porous carbon/GCE, and (-0.38 V , $-19.0 \mu\text{A}$) for MMO/PC/GCE were obtained. The bare/GCE gave a weak response indicating poor electrocatalytic ability due to slow electron transfer to FZD. Interestingly, the as-prepared MMO/PC/GCE exhibited the highest cathodic peak current compared to bare, MMO, and porous carbon electrodes respectively. Due to an open pore-like 3D porous carbon having a large active surface area with a nanoporous structure network combination with one-dimensional hybrid rods, it would enhance electronic conductivity between MMO/PC/GCE and FZD species at the electrode/solution interface and their synergy effect. The FZD detection of a reduction peak in the reverse scan and the lack of an oxidation peak demonstrated that the system is irreversible. This represents the reduction of the nitro group transformed into its hydroxylamine group with four electrons (4e^-) and four protons (4H^+) transfer reaction processes. Finally, the EIS and CV data demonstrate that MMO/PC/GCE is an effective and promising electrode material with strong catalytic activity for detecting FZD.

The electrocatalytic activity of the MMO/PC/GCE was evaluated by CV at a sweep rate of 50 mV/s in the presence of different concentrations of FZD ranging from 30 to 200 μM in 0.1 M PBS (pH-7). As shown in Figure 6A, the increasing FZD concentration resulted in a significant increase in cathodic peak current, it indicates the extraordinary electrocatalytic activity at the MMO/PC/GCE electrocatalyst. The corresponding calibration linear plot is displayed in Figure 6B, the linear plot between the concentration of FZD vs. cathodic current, yielding the following linear equation $I_{pc} [\mu\text{A}] = -0.092 [\mu\text{M}] - 9.350$, and the correlation coefficient $R^2 = 0.99$ respectively. The observed results prove that the as-prepared MMO/PC/GCE is electrocatalytic active sensing towards FZD.

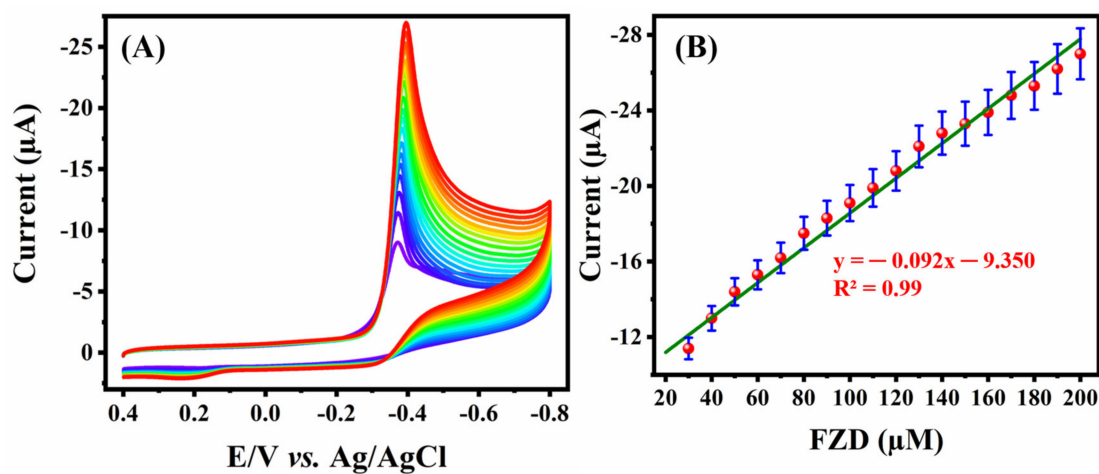


Figure 6. (A) CV responses for the progressive addition of FZD (30–200 μM) at MMO/PC/GCE in 0.1 M PBS (pH 7.0) at a sweep rate of 50 mV/s. (B) Calibration linear plot for the concentration of FZD vs. cathodic current (μA).

To investigate the reaction kinetic composite, the CV curve (Figure 7A) of MMO/PC/GCE in FZD 200 μM was observed at different scan speeds ranging from 20 to 300 mV/s. The obtained result shows that changing the scan rate linearly increases the cathodic current appropriately. The calibrated linear plot is shown in Figure 7B, the square root of scan rate vs. cathodic current (μA) with corresponding linear regression equation and correlation coefficient expressed as $I_{pc} = -3.855 (\nu)^{1/2} + 7.711$, $R^2 = 0.995$. It correctly identifies FZD reduction as a diffusion-controlled electron transfer mechanism on the surface of an MMO/PC/GCE.

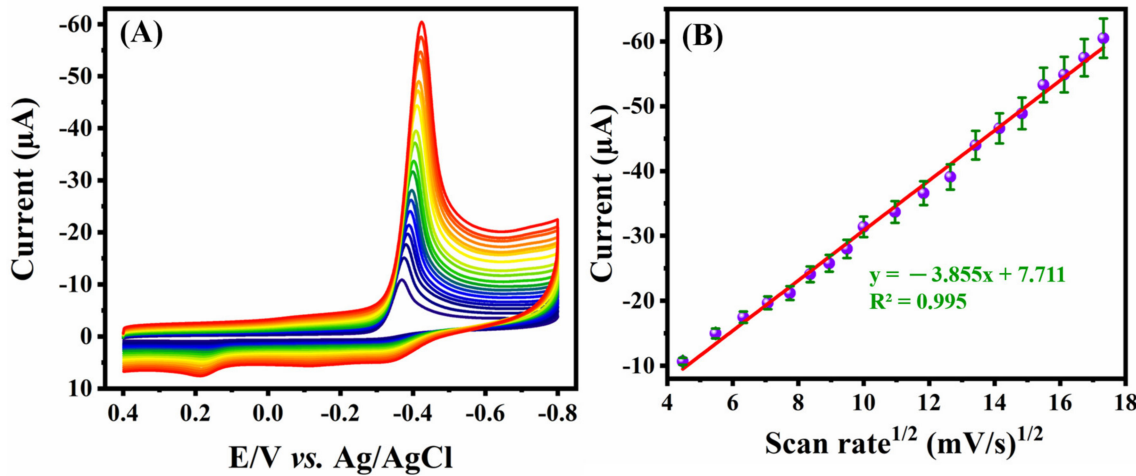


Figure 7. (A) CV responses for the linear scan rate of FZD 200 μM at MMO/PC/GCE in 0.1 M PBS (pH 7.0) with different scan rates at (20 to 300 mV/s). (B) Calibration plot for the square root of scan rate vs. cathodic current (μA).

Further, the CV method was conducted to analyze the electrochemical activity of the as-prepared MMO/PC/GCE under acidic to basic medium control. Figure 8A shows the CV curve exhibit for FZD 100 μM at pH (3,5,7,9,11) electrolyte medium on the MMO/PC/GCE at a sweep rate of 50 mV/s. It shows that at pHs 3.0 to 11.0, peak potential shifts towards more negative, also in the basic medium the peak current is reduced. Because the presence of additional hydroxide ions ($-\text{OH}$) may promote the further reduction of hydroxylamine ($-\text{NH}-\text{OH}$) into its equivalent nitroso ($-\text{NO}$) compound. Figure 8B shows the bar diagram of the pH 3.0–11.0 calculated cathodic peak current, this result suggested the maximum cathodic peak current attained at pH 7.0 (0.1 M PBS) neutral medium, which was selected as optimum for further experiments.

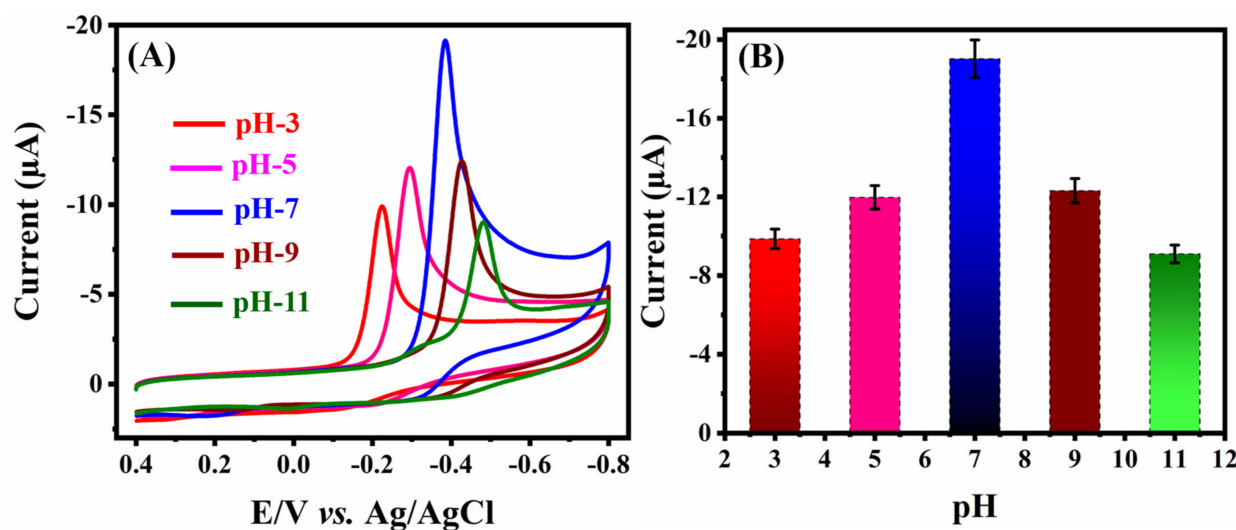


Figure 8. (A) The CV curve displayed in FZD 100 μM at pH (3,5,7,9,11) electrolyte medium on the MMO/PC/GCE at a sweep rate of 50 mV/s. (B) Corresponding bar diagram of the calculated CV of cathodic peak current.

2.2. Amperometric(*i-t*) Determination of FZD at MMO/PC Composite

The amperometric(*i-t*) current responses were obtained in a three-electrode system. The MMO/PC modified rotating ring disk (RRD) electrode as working electrode, Ag/AgCl as reference electrode, and platinum as counter electrode and 0.1 M PBS (pH-7.0) was used as electrolyte solution up to 10 min and N_2 gas saturated. The electrode input potential was held at -0.38 V, and the RRD electrode rotation speed was fixed at 1800 rpm. Figure 9A shows the amperometric(*i-t*) current response obtained for MMO/PC RRD electrode upon the successive addition of FZD various concentrations (1,10 mM) at every 50 sec interval. The obtained result revealed the cathodic current response increased with increasing FZD concentration. Additionally, the calculated steady-state current was less than 6 s, suggesting that the as-fabricated MMO/PC RRD electrode had a fast and highly sensitive response towards the reduction of FZD. Figure 9B shows (I and II) the linear range obtained for FZD detection from 150 nM to 41.05 μM and 41.05 to 471.05 μM with a regression equation of $I_{pc} = -0.100 [\mu\text{M}] - 1.108$; correlation coefficient $R^2 = 0.991$ and $I_{pc} = -0.024 [\mu\text{M}] - 4.486$; correlation coefficient $R^2 = 0.991$, respectively. The limit of detection and sensitivity was derived from the formula of ($\text{LOD} = 3\sigma/m$). Here, (σ) is the standard deviation of the steady-state current signal; (m) indicates a lower linear range slope value and the calculated results of LOD is 30 nM with an obtained sensitivity of $0.510 \mu\text{A} \mu\text{M}^{-1} \text{cm}^{-2}$ towards FZD. The MMO/PC hybrid composite electrode towards detection of FZD result is much better when compared previously reported and summarized in Table 1.

Table 1. Previously reported modified detection limit of FZD to compare to our result.

Modified Electrodes	Methods	Limit of Detection (μM)	Reference
Gr/Au/GCE	Amperometric	0.64	[49]
MWCNT/GCE	Cyclic voltammetry	2.3	[50]
Pt-Re NP/PAC/GCE	Linear sweep Voltammetry	0.075	[51]
MWCNT/GCE	Differential pulse voltammetry	0.08	[52]
MMO/PC/RRDE	Amperometric(<i>i-t</i>)	0.03	This Work

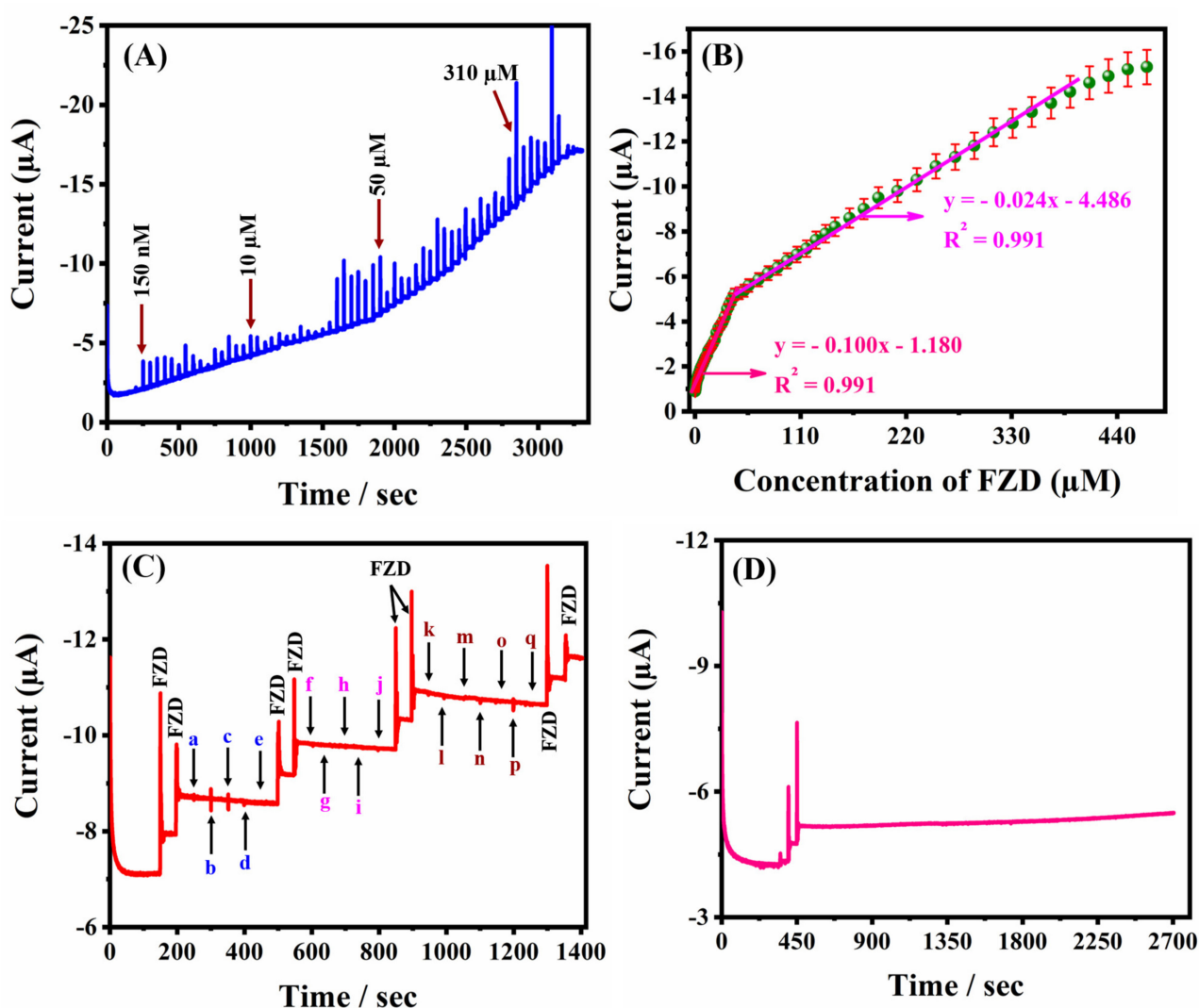


Figure 9. (A) Amperometric(i-t) responses of the MMO/PC modified RRD electrode to successive addition of FZD in an interval of every 50 s and electrolyte solution of 0.1 M PBS (pH 7.0) with input potential held at -0.38 V. (B) The linear calibration plot for concentration of FZD (μM) vs. cathodic current (μA). (C) The amperometric(i-t) current response of selectivity study for 100 μM FZD with equal amount of nitrocompounds ((a) nitrofurantoin (b) nimisulide (c) ornidazole (d) metronidazole (e) 2-nitroaniline), metal ions (f) Fe^{2+} , (g) Mg^{2+} , (h) pb^{2+} , (i) Zn^{2+} , (j) Na^{+} , and biological compounds (k) uric acid (l) isoniazid, (m) dopamine, (n) clorampinical, (o) fructose, (p) naproxen, and (q) glucose. (D) The MMO/PC modified RRD electrode examined operational stability test towards FZD 100 μM in 0.1 M PBS (pH 7.0) up to 2750 s.

2.3. Selectivity and Stability Test

The amperometric(i-t) test was performed to study selectivity test towards MMO/PC modified RRD electrode for FZD detection. The interferent species of nitro compounds ((a) nitrofurantoin (b) nimisulide (c) ornidazole (d) metronidazole (e) 2-nitroaniline), metal ions (f) Fe^{2+} , (g) Mg^{2+} , (h) pb^{2+} , (i) Zn^{2+} , (j) Na^{+} , and biological compounds (k) uric acid (l) isoniazid, (m) dopamine, (n) clorampinical, (o) fructose, (p) naproxen, and (q) glucose were added every 50 s of intervals in 0.1 M PBS (pH 7.0). As can be seen in Figure 9C, there is no significant current response except the FZD detection current. Therefore, the proposed sensor showed excellent anti-interference capability, and the as-fabricated MMO/PC modified RRD electrode proved highly selective to FZD sensing. The electrode stability test was carried out in the same experimental condition as the amperometric(i-t) steady-state current response by adding 100 μM FZD of the first three injections. The steady-state current response was detected up to 2750 s after the initial three additions of

FZD, and it retained 98% of its original current signal, as shown in Figure 9D. This result indicates as-prepared MMO/PC modified RRD electrode has excellent operation stability towards the detection of FZD.

2.4. Repeatability, Reproducibility, and Real-Sample Analysis

Figure 10A displays the MMO/PC/GCE, which have been employed to detect 200 μM FZD by CV consecutive four times to evaluate its repeatability. The relative standard deviation (RSD) of their CV current was calculated to be 1.32% which indicates MMO/PC/GCE has excellent retest reliability. To estimate, four individual MMO/PC/GCE were prepared and analyzed (Figure 10B). The calculated RSD value was 1.47%. This result demonstrates the as-fabricated MMO/PC composite has a good reproduction ability. In addition, the real-time monitoring analysis is performed by the amperometric(i-t) method.

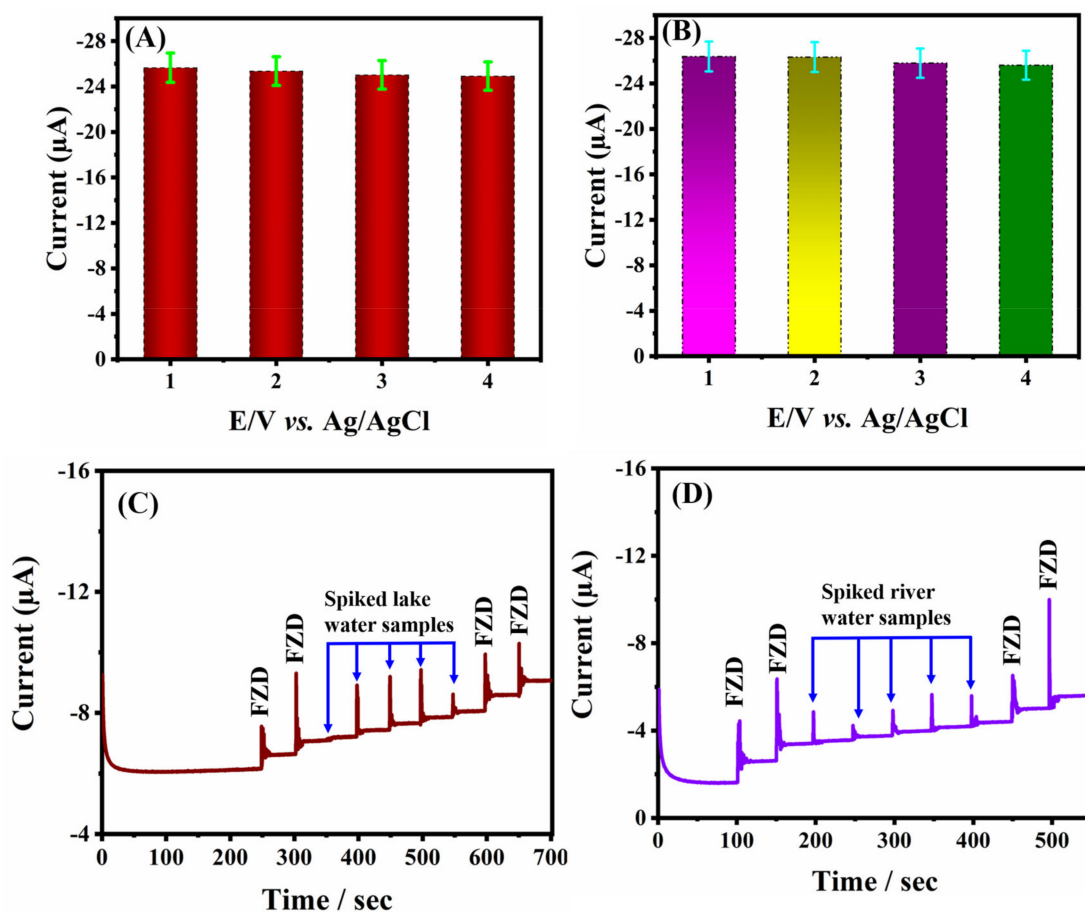


Figure 10. (A) The CVs curve of MMO/PC/GCE in the presence of 200 μM of FZD in repeatability test. (B) Four different MMO/PC/GCE were conducted for reproducibility tests. (C) Amperometric(i-t) responses of the MMO/PC modified RRD electrode to successive addition of lake water sample and (D) river water sample.

Real-sample analysis of the fabricated MMO/PC modified RRD electrode electrochemical sensor was investigated by detecting FZD in the lake and river water samples. In this experiment, river and lake water samples were obtained from the local area of Taipei City, Taiwan (ROC). The collected samples were filtered with a PVDF syringe filter. After that, the obtained samples were diluted with 0.1 M PBS (pH 7), then we conducted the electrochemical analysis. As shown in Figure 10C,D, the as-prepared MMO/PC modified RRD electrode was performed and spiked peaks are obtained. The obtained recovery result is given in Table 2, it is clearly indicated that the modified electrode has a potential application for the detection of FZD in environmental water samples. This validates the

accuracy of this approach and also demonstrates that the suggested electrochemical sensor has adequate dependability for determining FZD in environmental water samples.

Table 2. Real-time analysis of FZD in environmental samples.

Sample	Added (μM)	Found (μM)	Recovery (%)
Lake water	100	99.7	99.7
	110	109.5	99.5
	120	118.5	98.7
	130	129.5	99.6
	140	137.5	98.2
River water	22	21.8	99.0
	24	24.5	102.0
	26	25.5	98.2
	28	27.4	97.8
	30	30.5	101.6

3. Experimental

3.1. Chemical Reagent

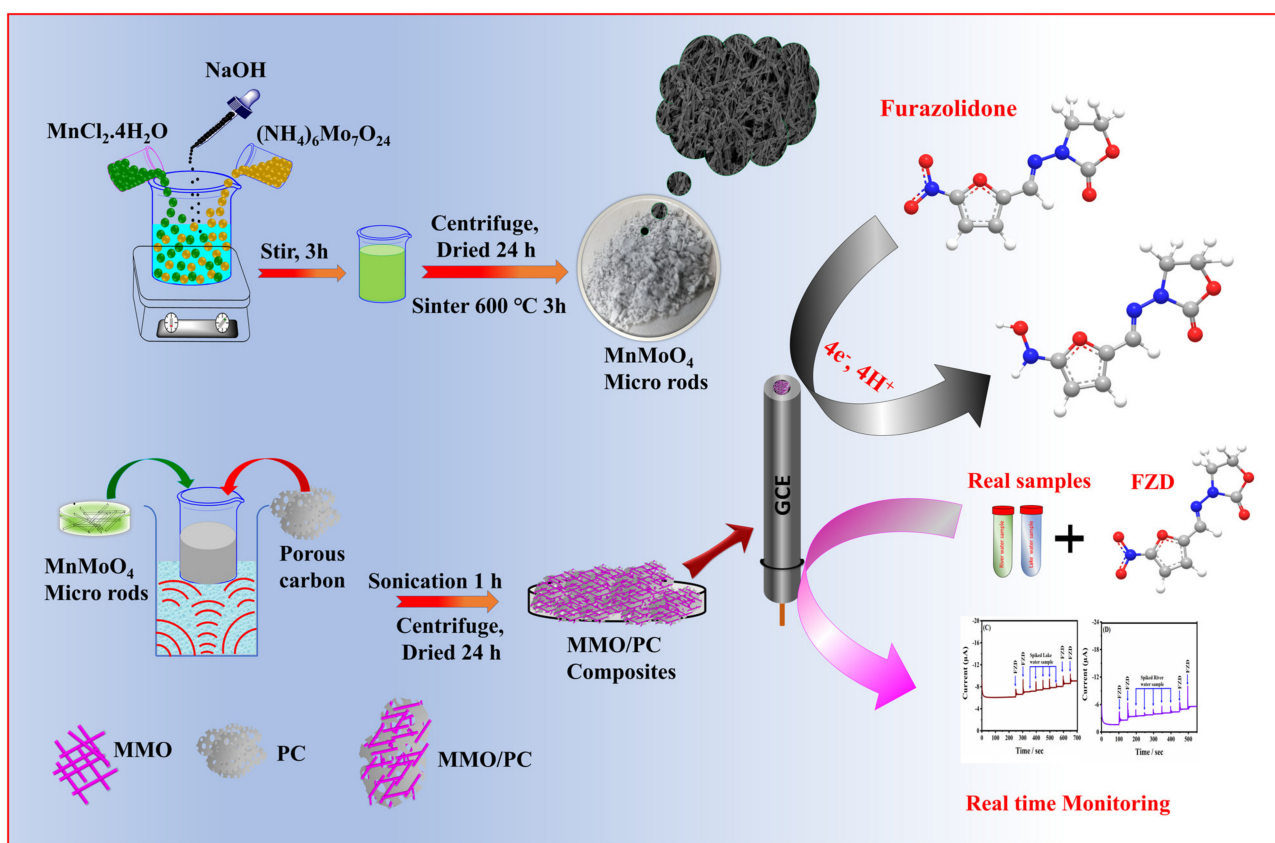
Manganese chloride tetrahydrate ($\text{MnCl}_2 \cdot 4\text{H}_2\text{O}$), ammonium heptamolybdate ($(\text{NH}_4)_6\text{Mo}_7\text{O}_{24}$), sodium hydroxide (NaOH), hydrochloric acid (HCl), monosodium phosphate monobasic monohydrate $\text{NaH}_2\text{PO}_5 \cdot \text{H}_2\text{O}$, sodium phosphate dibasic anhydrous Na_2HPO_4 , and all other chemicals were obtained from Sigma Aldrich Pvt. All chemical reagents were utilized without further purification. Deionized water (DI water-18.2 MΩ millipore) was used to synthesize and all electrolyte buffer solutions.

3.2. Synthesis Procedure of MMO Micro Rods

The facile co-precipitation method has been utilized for the synthesis of MnMoO_4 micro rods. Initially, manganese chloride tetrahydrate (0.18 g) and ammonium heptamolybdate (1.74 g) were combined separately with 30 DI water and constantly agitated for 30 min. The subsequently prepared two solutions were mixed dropwise one by one. Then, the stoichiometric sodium hydroxide solution was added to the above-mentioned mixing solution. The precipitate was formed and continuously stirred for up to 3 h. The obtained MnMoO_4 precipitate was centrifuged by washing with millipore DI water and ethanol several times. Continuously, the obtained product was dried at 50 °C in a heat oven for up to 24 h. Finally, the collected MnMoO_4 (denoted as MMO) powder was calcined in an air oven at 600 °C for up to 3 h.

3.3. Fabrication of MMO@PC Composite

Next up, MnMoO_4 micro rods assembled porous carbon composites were prepared through a wet chemical synthesis approach. The 50 mg MnMoO_4 micro rods and 10 mg porous carbon (PC) were added into the 10 mL (1:1 ratio of water and ethanol) solution. Then the mixture solution was ultrasonicated for 1 h (34/70 kHz frequency and 60 W power of ultrasonication at 20 °C). Afterward, the obtained solution was dried at 50 °C in a heat oven for 24 h. Finally, the collected MnMoO_4 micro rod assembled porous carbon composites (mentioned as MMO/PC composite) product was used for characterization. Scheme 1 represents the preparation of MMO/PC/GCE and the reduction mechanism of FZD processes.



Scheme 1. The schematic representation of synthesis and electrochemical reduction mechanism of FZD.

3.4. Preparation of MMO/PC/GCE

Before the modification processes, the blank GCE was pre-cleaned by 0.05 M alumina fine powder as stated in the draft. Then the blank GCE was washed with DI water, ethanol, and dried at room temperature. Then the as-prepared MMO/PC composite powder of about 1 mg was mixed with 1 mL of DI water. After, the solution was sonicated for 30 min. From that obtained solution, the 6 μ L slurry was dropped cast onto the mirror-like surface on the GCE. Then, the MMO/PC composite modified GCE was dried at ambient temperature. Finally, the obtained MMO/PC/GCE was performed for further electrochemical applications.

3.5. Characterization and Electrochemical Measurement

The powder X-ray diffraction (XRD, PANalytical X'pert PRO MRD, Almelo, Netherlands) with Cu K radiation ($\lambda = 0.15406$ nm) was used to examine the crystal structures of the as-prepared MMO/PC composite samples. Raman spectra were recorded with a micro-Raman Dongwoo Ramboss 500i with an incident laser at the wavelength of 514 nm. The X-ray photoelectron spectroscopy (XPS) experiment was undertaken on the surface composition of MMO/PC composite to investigate the chemical state of components. Field emission scanning electron microscopy (FESEM, JSM-7610F, JEOL, Tokyo, Japan) and high-resolution transmission electron microscopy were used to analyze the surface morphology of MMO micro rods and porous carbon (HR-TEM, Shimadzu JEM-1200 EXSTEM, Tokyo, Japan). The electronic conductivity and electron transfer activity of the as-prepared MMO/PC composite were investigated by electrochemical impedance spectroscopy (EIS), IM6ex ZAHNER instrument from Kronach, Germany. The electrocatalytic activity of the MMO/PC composite was investigated and measurement was carried out by CV (cyclic voltammetry; CHI1205A, and CHI 750A CH Instruments, Austin, TX, USA) and three-electrode system of glassy carbon electrode (GCE) as a working electrode (electrode

area = 0.07 cm²), Ag/AgCl was used as reference electrode and platinum electrodes used as the counter electrode.

4. Conclusions

The absence of inexpensive and reliable sensing instruments is making it difficult to evaluate water quality in environmental fluids. In this present work, we have prepared MMO micro rods that were synthesized in the co-precipitation method. The sonication assisted the MMO/PC and a composite was obtained. The as-prepared MMO/PC were characterized by XRD, RAMAN, XPS, FESEM, and HR-TEM. The as-prepared MMO/PC modified GCE was utilized for the highly sensitive and selective detection of FZD. As per CV results, the MMO/PC/GCE was showed a very good analytical performance in an optimized condition. The amperometric(i-t) method was utilized for the as-prepared MMO/PC modified RRD electrode resulting in a good linear range, lower LOD, higher stability, and reliability. The MMO/PC modified RRD electrode in practical application results exhibited good recovery obtained in environmental fluids. The proposed sensor is a significant step in developing a simple and low-cost method for detecting FZD in environment water resources on-site.

Author Contributions: S.M.B. designed the work, performed materials synthesis and characterization, and wrote the final draft; T.-W.C. contributed to review and editing the draft; S.-M.C. contributed in supervision, funding acquisition, review, and editing the draft; W.A.A.-O. contributed to review and editing the draft; A.M.A.-M. contributed to supervision, funding acquisition, review, and editing the draft. All authors have read and agreed to the published version of the manuscript.

Funding: This work was supported by the Minsitry of science and Technology of Taiwan, grant number MOST 110-2113-M-027-003 and APC was funded by project number (RSP-2021/247) King Saud University, Riyadh, Saudi Arabia.

Data Availability Statement: No new data were created or analyzed in this study.

Acknowledgments: The authors greatly acknowledge the Ministry of Science and Technology (MOST 110-2113-M-027-003), Taiwan. The authors extend their appreciation to the Researchers supporting project number (RSP-2021/247) King Saud University, Riyadh, Saudi Arabia.

Conflicts of Interest: The authors declare no conflict of interest.

References

1. Carignan, G.; Macintosh, A.I.; Sved, S. An Assay for Furazolidone Residues by Liquid Chromatography with Electrochemical Detection Applicable to Depletion Studies in Pigs. *J. Agric. Food Chem.* **1990**, *38*, 716–720. [[CrossRef](#)]
2. Xing, C.; Jing, X.; Zhang, X.; Yuan, J. Ultrasensitive indirect competitive ELISA and strip sensor for detection of furazolidone metabolite in animal tissues. *Food Agric. Immunol.* **2017**, *28*, 1269–1282. [[CrossRef](#)]
3. MacNeil, J.D. Drug residues in animal tissues. *J. AOAC Int.* **2001**, *84*, 191–193. [[CrossRef](#)]
4. Valadez-Salazar, A.; Guiscafre-Gallardo, H.; Sanchez-Garcia, S.; Muñoz, O. Detection of furazolidone in human biological fluids by high performance liquid chromatography. *J. Antimicrob. Chemother.* **1989**, *23*, 589–595. [[CrossRef](#)]
5. Botsoglou, N.A. Determination of furazolidone in eggs by high-performance liquid chromatography. *J. Agric. Food Chem.* **1988**, *36*, 1224–1227. [[CrossRef](#)]
6. Chu, P.S.; Lopez, M.I. Determination of nitrofuran residues in milk of dairy cows using liquid chromatography-tandem mass spectrometry. *J. Agric. Food Chem.* **2007**, *55*, 2129–2135. [[CrossRef](#)]
7. Diblikova, I.; Cooper, K.M.; Kennedy, D.G.; Franek, M. Monoclonal antibody-based ELISA for the quantification of nitrofuran metabolite 3-amino-2-oxazolidinone in tissues using a simplified sample preparation. *Anal. Chim. Acta* **2005**, *540*, 285–292. [[CrossRef](#)]
8. Jain, A.K.; Singh, K.P. Evaluation of Antibacterial Studies in Harsingar. *Int. Res. J. Pharm.* **2013**, *4*, 151–153. [[CrossRef](#)]
9. Squella, J.; Bollo, S.; Nunez-Vergara, L. Recent Developments in the Electrochemistry of Some Nitro Compounds of Biological Significance. *Curr. Org. Chem.* **2005**, *9*, 565–581. [[CrossRef](#)]
10. Klingler, R.J.; Kochi, J.K. Electron-transfer kinetics from cyclic voltammetry. Quantitative description of electrochemical reversibility. *J. Phys. Chem.* **1981**, *85*, 1731–1741. [[CrossRef](#)]
11. Aristov, N.; Habekost, A. Cyclic Voltammetry-A Versatile Electrochemical Method Investigating Electron Transfer Processes. *World J. Chem. Educ.* **2015**, *3*, 115–119. [[CrossRef](#)]

12. Karuppiah, C.; Muthupandi, K.; Chen, S.M.; Ali, M.A.; Palanisamy, S.; Rajan, A.; Prakash, P.; Al-Hemaid, F.M.A.; Lou, B.S. Green synthesized silver nanoparticles decorated on reduced graphene oxide for enhanced electrochemical sensing of nitrobenzene in waste water samples. *RSC Adv.* **2015**, *5*, 31139–31146. [[CrossRef](#)]
13. Terbouche, A.; Lameche, S.; Ait-Ramdane-Terbouche, C.; Guerniche, D.; Lerari, D.; Bachari, K.; Hauchard, D. A new electrochemical sensor based on carbon paste electrode/Ru(III) complex for determination of nitrite: Electrochemical impedance and cyclic voltammetry measurements. *Meas. J. Int. Meas. Confed.* **2016**, *92*, 524–533. [[CrossRef](#)]
14. Karimi-Maleh, H.; Fakude, C.T.; Mabuba, N.; Peleyeju, G.M.; Arotiba, O.A. The determination of 2-phenylphenol in the presence of 4-chlorophenol using nano-Fe₃O₄/ionic liquid paste electrode as an electrochemical sensor. *J. Colloid Interface Sci.* **2019**, *554*, 603–610. [[CrossRef](#)] [[PubMed](#)]
15. Karimi-Maleh, H.; Arotiba, O.A. Simultaneous determination of cholesterol, ascorbic acid and uric acid as three essential biological compounds at a carbon paste electrode modified with copper oxide decorated reduced graphene oxide nanocomposite and ionic liquid. *J. Colloid Interface Sci.* **2020**, *560*, 208–212. [[CrossRef](#)] [[PubMed](#)]
16. Karuppiah, C.; Velmurugan, M.; Chen, S.M.; Devasenathipathy, R.; Karthik, R.; Wang, S.F. Electrochemical Activation of Graphite Nanosheets Decorated with Palladium Nanoparticles for High Performance Amperometric Hydrazine Sensor. *Electroanalysis* **2016**, *28*, 808–816. [[CrossRef](#)]
17. Saleh, M.M.; Marzi, K.E.; Naghian, E.; Homayoun, K.A.; Sohouli, E.; Plonska-Brzezinska, M.E.; Ali, S.N.; Rahimi-Nasrabadi, M.; Ahmadi, F. Application of carbon nanoion-NiMoO₄-MnWO₄ nanocomposite for modification of glassy carbon electrode: Electrochemical determination of ascorbic acid. *Microchem. J.* **2020**, *159*, 105470. [[CrossRef](#)]
18. Guo, S.; Dong, S. Biomolecule-nanoparticle hybrids for electrochemical biosensors. *TrAC Trends Anal. Chem.* **2009**, *28*, 96–109. [[CrossRef](#)]
19. Qiu, J.D.; Shi, L.; Liang, R.P.; Wang, G.C.; Xia, X.H. Controllable deposition of a platinum nanoparticle ensemble on a polyani-line/graphene hybrid as a novel electrode material for electrochemical sensing. *Chem. A Eur. J.* **2012**, *18*, 7950–7959. [[CrossRef](#)]
20. Zhao, X.H.; Ma, S.N.; Long, H.; Yuan, H.; Tang, C.Y.; Cheng, P.K.; Tsang, Y.H. Multifunctional Sensor Based on Porous Carbon Derived from Metal-Organic Frameworks for Real Time Health Monitoring. *ACS Appl. Mater. Interfaces* **2018**, *10*, 3986–3993. [[CrossRef](#)]
21. Yang, Y.; Chiang, K.; Burke, N. Porous carbon-supported catalysts for energy and environmental applications: A short review. *Catal. Today* **2011**, *178*, 197–205. [[CrossRef](#)]
22. Kitano, M.; Arai, K.; Kodama, A.; Kousaka, T.; Nakajima, K.; Hayashi, S.; Hara, M. Preparation of a sulfonated porous carbon catalyst with high specific surface area. *Catal. Letters* **2009**, *131*, 242–249. [[CrossRef](#)]
23. Bhadra, B.N.; Song, J.Y.; Uddin, N.; Khan, N.A.; Kim, S.; Choi, C.H.; Jhung, S.H. Oxidative denitrogenation with TiO₂@porous carbon catalyst for purification of fuel: Chemical aspects. *Appl. Catal. B Environ.* **2019**, *240*, 215–224. [[CrossRef](#)]
24. Gopalakrishnan, A.; Badhulika, S. Sulfonated porous carbon nanosheets derived from oak nutshell based high-performance supercapacitor for powering electronic devices. *Renew. Energy* **2020**, *161*, 173–183. [[CrossRef](#)]
25. Veerakumar, P.; Sangili, A.; Manavalan, S.; Thanasekaran, P.; Lin, K.C. Research Progress on Porous Carbon Supported Metal/Metal Oxide Nanomaterials for Supercapacitor Electrode Applications. *Ind. Eng. Chem. Res.* **2020**, *59*, 6347–6374. [[CrossRef](#)]
26. Imshennik, V.K.; Suzdalev, I.P.; Stavinskaya, O.N.; Shklovskaya, N.I.; Schünemann, V.; Trautwein, A.X.; Winkler, H. Preparation and characterization of porous carbon loaded with iron particles: A possible magnetic carrier of medical drugs. *Microporous Mater.* **1997**, *10*, 225–230. [[CrossRef](#)]
27. Fellinger, T.P.; Hasché, F.; Strasser, P.; Antonietti, M. Mesoporous nitrogen-doped carbon for the electrocatalytic synthesis of hydrogen peroxide. *J. Am. Chem. Soc.* **2012**, *134*, 4072–4075. [[CrossRef](#)]
28. Zhang, Y.; Huang, J.; Liao, Z.; Hu, A.; Li, X.; Saito, N.; Zhang, Z.; Yang, L.; Hirano, S.I. Natural Self-Confined Structure Effectively Suppressing Volume Expansion toward Advanced Lithium Storage. *ACS Appl. Mater. Interfaces* **2021**, *24*, 24634–24642. [[CrossRef](#)]
29. Chen, T.; Fu, Y.; Liao, W.; Zhang, Y.; Qian, M.; Dai, H.; Tong, X.; Yang, Q. Fabrication of Cerium-Doped CoMoP/MoP@C Heterogeneous Nanorods with High Performance for Overall Water Splitting. *Energy Fuels* **2021**, *35*, 14169–14176. [[CrossRef](#)]
30. Minakshi, M.; Barmi, M.J.; Jones, R.T. Rescaling metal molybdate nanostructures with biopolymer for energy storage having high capacitance with robust cycle stability. *Dalt. Trans.* **2017**, *46*, 3588–3600. [[CrossRef](#)]
31. Jiang, L.; Wang, Z.; Chen, H.; Chen, Y.; Chen, P.; Xu, Z. Thermal annealing effects on the luminescence and scintillation properties of CaMoO₄ single crystal grown by Bridgman method. *J. Alloys Compd.* **2018**, *734*, 179–187. [[CrossRef](#)]
32. Karthika, A.; Nikhil, S.; Suganthi, A.; Rajarajan, M. A facile sonochemical approach based on graphene carbon nitride doped silver molybdate immobilized nafion for selective and sensitive electrochemical detection of chromium (VI) in real sample. *Adv. Powder Technol.* **2020**, *31*, 1879–1890. [[CrossRef](#)]
33. Yaghoubian, H.; Tajik, S.; Beitollahi, H.; Sarhadi, H.; Sheikhshoae, I. Fe₂MoO₄ magnetic nanocomposite modified screen printed graphite electrode as a voltammetric sensor for simultaneous determination of nalbuphine and diclofenac. *J. Mater. Sci. Mater. Electron.* **2021**, *32*, 17311–17323. [[CrossRef](#)]
34. Du, D.; Lan, R.; Xu, W.; Beanland, R.; Wang, H.; Tao, S. Preparation of a hybrid Cu₂O/CuMoO₄ nanosheet electrode for high-performance asymmetric supercapacitors. *J. Mater. Chem. A* **2016**, *4*, 17749–17756. [[CrossRef](#)]
35. Liu, M.C.; Kong, L.B.; Lu, C.; Ma, X.J.; Li, X.M.; Luo, Y.C.; Kang, L. Design and synthesis of CoMoO₄-NiMoO₄·xH₂O bundles with improved electrochemical properties for supercapacitors. *J. Mater. Chem. A* **2013**, *1*, 1380–1387. [[CrossRef](#)]

36. Ramkumar, R.; Minakshi, M. Fabrication of ultrathin CoMoO₄ nanosheets modified with chitosan and their improved performance in energy storage device. *Dalt. Trans.* **2015**, *44*, 6158–6168. [[CrossRef](#)]
37. Li, H.; Xuan, H. Hierarchical design of Ni(OH)₂/MnMoO₄ composite on reduced graphene oxide/Ni foam for high-performances battery-supercapacitors hybrid device. *Int. J. Hydrogen Energy* **2021**, *46*, 38198–38211. [[CrossRef](#)]
38. Hussain, S.; Khan, A.J.; Arshad, M.; Javed, M.S.; Ahmad, A.; Ahmad, S.S.S.; Khan, M.R.; Akram, S.; Zulfiqar; Ali, S.; et al. Charge storage in binder-free 2D-hexagonal CoMoO₄ nanosheets as a redox active material for pseudocapacitors. *Ceram. Int.* **2021**, *47*, 8659–8667. [[CrossRef](#)]
39. Zhang, J.; Hou, Q.; Chang, J.; Zhang, D.; Peng, Y.; Yang, X. Improvement of hydrogen storage performance of MgH₂ by MnMoO₄ rod composite catalyst. *Solid State Sci.* **2021**, *121*, 106750. [[CrossRef](#)]
40. Venkatesh, K.; Rajakumaran, R.; Chen, S.M.; Karuppiah, C.; Yang, C.C.; Ramaraj, S.K.; Ali, M.A.; Al-Hemaid, F.M.A.; El-Shikh, M.S. A novel hybrid construction of MnMoO₄ nanorods anchored graphene nanosheets; an efficient electrocatalyst for the picomolar detection of ecological pollutant ornidazole in water and urine samples. *Chemosphere* **2021**, *273*, 129665. [[CrossRef](#)]
41. Ranjith, K.S.; Ezhil Vilian, A.T.; Ghoreishian, S.M.; Umapathi, R.; Hwang, S.-K.; Oh, C.W.; Huh, Y.S.; Han, Y.-K. Hybridized 1D–2D MnMoO₄–MXene nanocomposites as high-performing electrochemical sensing platform for the sensitive detection of dihydroxybenzene isomers in wastewater samples. *J. Hazard. Mater.* **2022**, *421*, 126775. [[CrossRef](#)] [[PubMed](#)]
42. Mai, L.Q.; Yang, F.; Zhao, Y.L.; Xu, X.; Xu, L.; Luo, Y.Z. Hierarchical MnMoO₄/CoMoO₄ heterostructured nanowires with enhanced supercapacitor performance. *Nat. Commun.* **2011**, *2*, 1–5. [[CrossRef](#)] [[PubMed](#)]
43. Huang, W.; Zhang, H.; Huang, Y.; Wang, W.; Wei, S. Hierarchical porous carbon obtained from animal bone and evaluation in electric double-layer capacitors. *Carbon, N.Y.* **2011**, *49*, 838–843. [[CrossRef](#)]
44. Ghosh, D.; Giri, S.; Moniruzzaman, M.; Basu, T.; Mandal, M.; Das, C.K. α MnMoO₄/graphene hybrid composite: High energy density supercapacitor electrode material. *Dalt. Trans.* **2014**, *43*, 11067–11076. [[CrossRef](#)] [[PubMed](#)]
45. Chen, H.; Wang, G.; Chen, L.; Dai, B.; Yu, F. Three-Dimensional Honeycomb-Like Porous Carbon with Both Interconnected Hierarchical Porosity and Nitrogen Self-Doping from Cotton Seed Husk for Supercapacitor Electrode. *Nanomaterials* **2018**, *8*, 412. [[CrossRef](#)]
46. Cao, Y.; Li, W.; Xu, K.; Zhang, Y.; Ji, T.; Zou, R.; Yang, J.; Qin, Z.; Hu, J. MnMoO₄·4H₂O nanoplates grown on a Ni foam substrate for excellent electrochemical properties. *J. Mater. Chem. A* **2014**, *2*, 20723–20728. [[CrossRef](#)]
47. Saravanan Kumar, B.; Ramachandran, S.P.; Ravi, G.; Ganesh, V.; Sakunthala, A.; Yuvakkumar, R. Transition mixed-metal molybdates (MnMoO₄) as an electrode for energy storage applications. *Appl. Phys. A Mater. Sci. Process.* **2019**, *125*, 1–11. [[CrossRef](#)]
48. Rong, X.; Qiu, F.; Qin, J.; Zhao, H.; Yan, J.; Yang, D. A facile hydrothermal synthesis, adsorption kinetics and isotherms to Congo Red azo-dye from aqueous solution of NiO/graphene nanosheets adsorbent. *J. Ind. Eng. Chem.* **2015**, *26*, 354–363. [[CrossRef](#)]
49. He, B.S.; Du, G.A. A simple and sensitive electrochemical detection of furazolidone based on an Au nanoparticle functionalized graphene modified electrode. *Anal. Methods* **2017**, *9*, 4341–4348. [[CrossRef](#)]
50. Fotouhi, L.; Nemati, M.; Heravi, M.M. Electrochemistry and voltammetric determination of furazolidone with a multi-walled nanotube composite film-glassy carbon electrode. *J. Appl. Electrochem.* **2011**, *41*, 137–142. [[CrossRef](#)]
51. Veerakumar, P.; Sangili, A.; Chen, S.M.; Pandikumar, A.; Lin, K.C. Fabrication of Platinum-Rhenium Nanoparticle-Decorated Porous Carbons: Voltammetric Sensing of Furazolidone. *ACS Sustain. Chem. Eng.* **2020**, *8*, 3591–3605. [[CrossRef](#)]
52. DUAN, L.; ZHANG, L. Electrochemical Behavior of Furazolidone at Mulit-walled Carbon Nanotubes Modified Glassy Carbon Electrode and Its Analytical Application. *J. Anal. Sci.* **2012**, *5*, 673–676.